

Title: High-Throughput Phenotyping of Drought-Stress and Fusarium Wilt in Lettuce Using UAV-Based Thermography

Project Type: Type I

Principal Investigator: Duke Pauli, PhD, School of Plant Sciences, University of Arizona

Project Period: August 1st, 2019 through June 22, 2020

1. Introduction

Lettuce is an economically important crop that is prized for its culinary versatility and known health benefits. But as with all crops, lettuce is threatened by abiotic stressors such as lack of water as well as biotic stresses such as Fusarium wilt (*Fusarium oxysporum*). Both of these plant stressors are likely to increase in frequency as demand for freshwater continues to heighten while the occurrence of Fusarium in production fields becomes more common. To address these challenges, new technologies must be developed that can detect and quantify the presence of stress in lettuce fields so that appropriate management decisions can be made.

Remote thermal imaging, also known as thermography, provides a rapid way to identify plant stresses associated with a reduction in plant-water content. As plant-water content decreases, the effect of evaporative cooling via transpiration is reduced leading to a distinct increase in plant temperature relative to plants with optimal hydration. The reduction in plant-water content can occur via two mechanisms encountered in production fields; reduced supplies of soil water that plants can access (drought), or reduced movement of water through the plant caused by blocked or damaged xylem, which is the exact pathogenesis of Fusarium wilt.

Many studies have demonstrated that small unoccupied aircraft systems (sUAS) can serve as highly efficient tools for collecting data on crop fields. However, it is necessary that a study be conducted to test and optimize thermography for its ability to phenotype abiotic and biotic stress in lettuce at field scale. To that end, a sUAS outfitted with a thermographic camera can be used to rapidly phenotype entire fields and identify drought-stressed or heavily diseased areas. Phenotypic data processed and extracted in this manner can also be used for downstream analyses, such as the identification of genes controlling the plant's response to these stressors that will aid improvement of lettuce in the future.

Finally, it is crucial that tools are developed that can benefit both researchers and producers as finding solutions to these problems is a community challenge. There are many potential research directions that can stem from the proposed study, and it will serve as an excellent starting point from which to investigate other phenotypes in lettuce or other leafy crops. For this work, we evaluated the application of thermography to cotton and lettuce production as these are two critical crops for Arizona agriculture. The work with cotton was to assess the ability of thermal imagery to capture changes in plant available water due to varied irrigation methods, representing different levels of water deficit, in a controlled experiment. The preliminary work performed in lettuce was to assess if Fusarium-infected lettuce heads could be visually detected in thermal imagery in a production environment.

2. Methods

2.1 Imaging System

Thermal image data was collected with an sUAS (Matrice 600 Pro, DJI, Shenzhen, China) equipped with a thermal infrared imaging system. The system consisted of a camera (Tau 2, Teledyne FLIR, Wilsonville, OR), camera housing (ThermalCapture 2.0 640, TeAx Technology

GmbH, Germany), and custom gimbal (TeAx 2-Axis Brushless Gimbal, TeAx Technology GmbH, Germany). The thermal imaging system had a pixel resolution of 640×512 and a thermal resolution of $\pm 2.0^\circ\text{C}$. Images were captured on a continuous basis generating a video file (TMC file type), however, an onboard bin file written to the SD card extracts individual image frames at a rate of 1 Hz. The extracted images constitute a compressed video file which is used for downstream processing. Prior to the start of the flight, the camera was allowed to acclimate for 20 minutes to ambient environmental conditions. Days with low wind and cloud cover, as well as days furthest from the previous irrigation event, were targeted for each flight.

2.2 Fields and flights

2.2.1 Maricopa field trials assessing water stress assessment using thermography

The Maricopa field experiment conducted for this work, including design, crop and irrigation management, and soil properties mapping has been described extensively in (Thorp et al. 2022), but will be briefly summarized. The experiment was conducted at The University of Arizona's Maricopa Agricultural Center located in Maricopa, AZ, USA (33.079°N , 111.977°W , elevation of 360 m) during the 2020 cotton growing season. Four irrigation management treatments, described below, were evaluated using a randomized block design consisting of six replicated blocks and totaling 24 plots (experimental units). Each plot measured 24.4 m wide, translating to 24 planted cotton rows with an inter-row spacing of 101.6 cm, by 36 m in length. For further geospatial analyses and irrigation treatment applications, each plot was divided into 24 subplots with dimensions of 6×6 m. This field design required 2.8 ha of land. The field was planted on April 18, 2020 [day of year (DOY) 109] with upland cotton (*Gossypium hirsutum* L., cv. 'NexGen 5007 B2XF', Americot, Inc., Lubbock, TX) using a vacuum planter (Monosem, Largeasse, France). Standard cultivation and management practices for cotton production in the Southwest were followed.

The irrigation treatments were as follows: Model (MDL) – determined irrigation amount solely by using the FAO-56 dual crop coefficient irrigation model. Drone (DRN) – determined irrigation amount by using FAO-56 model but added spatial crop cover data derived from a sUAS to achieve more accurate water availability estimates. Soil (SOL) – used spatial data for soil water holding limits in conjunction with the model to calculate the irrigation estimate. Variable Rate Index (VRI) – used VRI technology for site-specific irrigation in conjunction with the irrigation model to calculate the estimate.

A total of 13 flights were collected from 30 June 2020 (DOY 182) to 23 September 2020 (DOY 267). Flight planning software (Pix4DCapture, Pix4D SA, Lausanne, Switzerland) was used to establish a grid flight pattern with image overlap, both forward and lateral, set at 90%. Flights were conducted at solar noon and at an altitude of 50 m resulting in a ground sampling resolution of 6.54 cm/pixel; total mission time was approximately 24 minutes to cover the field site with dimensions 184×188 m.

Ground control points (GCPs) were constructed and positioned around the field, for both the Maricopa and Yuma flights, which allowed the collected images to be georectified upon stitching, to form a georeferenced orthomosaic. The GCPs were constructed using 0.1016 cm thick 5052 Aluminum alloy sheet, $2.54 \times 60.96 \times 60.96$ cm piece extruded Polystyrene (XPS) foamboard, and $0.25 \times 60.96 \times 60.96$ cm sheet of medium-density fiberboard. These materials were chosen to maximize the temperature contrast to allow for clear identification in the collected images. There were seven GCPs placed on the north side of the field and seven GCPs placed on the south side of the field.

To provide ground-truthed temperature references, several objects were placed within the area imaged by sUAS. These included coolers containing ice, eight cinder blocks arranged in a 4 × 2 block pad measuring dimensions of 81.3 × 81.3 × 20.3 cm, a 78.0 × 82.0 cm aluminum rectangle with center cutout placed on the dirt road adjacent the field, and selected cotton plants next to the ground truth objects. During the sUAS flight, temperature of the items were measured using handheld infrared thermometers (Mastercool, 52224-A-SP, Randolph, NJ), and were taken four times during the flight. The temperature of the XPS foam board portion of the GCP closest to the other ground truth objects was also recorded.

2.2.2 Yuma field trials investigating ability to detect Fusarium infection in-field

Given the duration from funding to acquisition of equipment, assembly of drone imaging system, and camera calibration, we were unable to acquire data on the YCEDA-hosted Fusarium trials that occurred in 2019. Instead, we worked with Dr. Silinski on imaging grower fields where the presence of Fusarium-infected heads had been documented. Two flights were conducted on 23 November 2020 (DOY 328) and 20 November 2021 (DOY 324). A grid flight pattern with image overlap, both forward and lateral, set at 85% was used. Flights were conducted at an altitude of 15 m and 20 m resulting in a ground sampling resolution of 1.96 and 2.62 cm/pixel, respectively. Total mission time was approximately eight and 15 minutes with dimensions 28 × 139 and 75 × 136 m for flights conducted in 2020 and 2021, respectively.

Prior to the capture of thermal imagery, an RGB flight was conducted using a Phantom 4 Pro V2 drone (DJI, Shenzhen, China). A grid flight pattern with image overlap of 85% in both the forward and lateral directions was used. Flights were conducted at an altitude of 15 m and 20 m to match the thermal flights. The total mission time was approximately eight and 15 minutes for flights conducted in 2020 and 2021, respectively.

In 2020, manual canopy temperature measurements were taken of both healthy lettuce heads and those suspected of being diseased using a handheld infrared thermometer (FLIR TG 165, FLIR Systems Inc., USA). Measurements were taken with the user standing upright, their arm fully extended at a 45 degree angle to their body, and the thermometer pointing at the center of the lettuce head. The measurement was also taken in a manner that would not cast a shadow on the plants. This methodology was conducted for all manual measurements with the handheld infrared thermometer to ensure consistency.

2.3 Data processing

2.3.1 Camera Calibration

Prior to the start of the growing season, the thermal camera was calibrated using a temperature controlled room located at the USDA Arid Land Agricultural Research Center (ALARC) research station in Maricopa, AZ. A blackbody (CES100-06/CF/VG, Electro Optical Industries, Santa Barbara, California) was set up in a temperature controlled room and set to the room temperature. Once the blackbody and room temperature was stable, three images of the blackbody were taken using the thermal camera. This step was repeated at 13 different blackbody temperatures ranging from 5°C to 65°C. Images of the blackbody were taken at eight different room temperatures ranging from 5°C to 45°C. During this process, the focal plane array temperature was collected and used to establish eight calibration curves. These eight curves represent the calibration room temperatures at which the blackbody temperatures were set across the selected 13 temperatures. The curves were used to interpolate pixel values from digital number (DN) to degrees Celsius.

Temperatures of the blackbody under each of the calibration room temperatures were imported into Python (version 3.8) where a linear regression, using 'scikit-learn' (Pedregosa et al. 2012), was performed to establish a general relationship between blackbody temperature (°C) and digital number (DN). The uncalibrated image was imported into Python, using 'Pillow' (Dev n.d.), and the established linear equation was used to convert the uncalibrated image pixel array to degrees celsius. The metadata from the uncalibrated image was then associated to the calibrated pixel array, using the 'piexif' library in Python (Piexif, 2015), rendering a calibrated image that could be used for further processing.

2.3.2 Image processing and temperature extraction

Upon completion of the sUAS thermal flight, the raw TMC video file was uploaded to the ThermoViewer software, version 3.7 (TeAx Technology GmbH, Germany) so that raw, individual TIFF images, with data represented as digital numbers, could be exported along with corresponding image metadata contained in a CSV file. Once single images were exported from the ThermoViewer software, the digital numbers were converted to temperature values (degree Celsius) using the above described calibration model to generate thermal images for further processing and analyses.

The calibrated thermal images were next imported into Pix4D Mapper for post processing. Initial steps of processing included selecting the correct camera model ("ThermalCapture_13.0_640x512 (Grayscale)", geospatial coordinate system ("WGS 84/UTM zone 12N"), and processing template ("Thermal Camera"). Image stitching was completed in the following order based on Pugh, Thorp, and Gonzalez 2021 (a) key points were extracted using image scale set to "Full" so a tie point cloud could be generated and internal parameters optimization to 'All Prior' since images were calibrated before the orthomosaic processing; (b) quality reports were assessed to make sure image stitching was acceptable based on the number of images used, key points used for image alignment, camera optimization, and the median number of matches per calibrated image; (c) ground control point (GCPs) positions, measured with a cm-level accuracy using real-time kinematic GPS system (model 5800, Trimble Inc., Sunnyvale, CA), were imported and manually selected to georeference the images containing GCPs; (d) reoptimization and matching among the remaining images was completed to create georeferenced orthomosaic; and (e) generation of a reflectance map of the orthomosaic based on individual pixel reflectance representing temperature (in °C).

No GCPs were set out during the flights conducted in Yuma as we do not possess a portable RTK trimble system. With no defined points in the field to reference we are unable to produce a georeferenced orthomosaic, which limits our ability to process the images in an automated fashion.

2.3.2.1 Maricopa

To extract plant canopy temperatures from the georeferenced reflectance orthomosaic, the following workflow was carried out for each individual date that data were collected. First, the full field orthomosaic was clipped to remove extraneous objects from the scene (vehicles, roads, etc.) to reduce data artifacts and provide an orthomosaic consisting of plants and soil. Using the entire orthomosaic, a histogram of pixel values was created that exhibited a clear bimodal distribution representing plant and soil pixels. Next, k-means clustering, implemented in 'OpenCV' (Bradski 2000), was used to find the local maxima of each mode within the bimodal distribution with these values representing the mean temperatures for plant and soil pixels. With these points defined, the local minima between them was determined and used as the threshold

to classify pixels as either “plant” or “soil.” To generate subplot-level plant canopy temperature values, a custom Python script (Van Rossum & Drake, 2009), which uses a manually developed GeoJSON shape file (QGIS.org, 2023) to demarcate plot boundaries, was used to extract plant temperatures from the georeferenced reflectance orthomosaic using the determined classification threshold. In an effort to mitigate pixel contamination, plant canopy temperature was extracted by generating a mean using the lowest 33% of plant pixel values comparable to previous studies (Bian et al. 2019).

2.3.2.2 Yuma

To extract plant canopy temperatures from the non-georeferenced orthomosaic, the following workflow was carried out. First, visual assessment of the orthomosaic was carried out to identify symptomatic lettuce heads. The location of interest was confirmed to exhibit disease symptoms through manual validation using the complimentary RGB imagery collected on the same day. Once confirmed, the naively stitched thermal orthomosaic was loaded into QGIS and the “identify features” tool was used to extract individual pixel temperature values. Once extracted, a manual comparison of symptomatic and non-symptomatic plant temperature was conducted.

3. Results

3.1 MAC results

To validate the ability of the sUAS thermal setup to detect differences in plant canopy temperature due to differences in irrigation, a correlation analysis was performed. A negative correlation was observed between irrigation and plant canopy temperature with values ranging between -0.31 and -0.74, with the lowest and highest correlation values produced on DOY 182 and 224, respectively (Appendix I, Figure 1). Correlations between irrigation and plant canopy temperature were significant for all dates flown (Appendix I, Figure 1).

To further illustrate the effect of irrigation on plant canopy temperature, plant canopy temperature and irrigation values were compared between an early (DOY 182) and late (DOY 224) treatment flight (Appendix I, Figure 2). MDL and SOL treatments were cumulatively irrigated 10.7 mm more than VRI and DRN treatments when the early treatment flight was conducted with differences in plant canopy exhibiting a 0.5°C difference. During the late treatment flight, MDL and SOL treatments were cumulatively irrigated 105.94 mm more than VRI and DRN treatments exhibiting a 3.1°C difference in plant canopy temperature.

3.2 Preliminary results from Yuma work

As mentioned previously, we were unable to collect data on the YCEDA-hosted Fusarium trials hosted in 2019 due to the duration of time it took to acquire, assemble, and validate the sUAS thermal imaging system. However, we were able to carry out testing of the thermal sUAS in 2020 and 2021 on grower fields with Fusarium-infected lettuce heads present. During these evaluations, we conducted both RGB and thermal imaging flights to assess the ability of the thermography to identify Fusarium-infected heads based on differences in lettuce head temperature.

Using a handheld IRT, lettuce head temperatures were taken in an effort to detect differences in temperature between healthy and symptomatic heads in 2020. Temperatures were 28.37°C and 31.73°C on average for healthy and symptomatic lettuce heads. Along with the manual IRT temperatures, efforts to identify diseased heads using thermal imagery were successful

(Appendix I, Figure 3). Similar trends were found when comparing healthy and symptomatic heads in the 2021 thermal imagery. Healthy heads exhibited lower temperatures when compared to symptomatic heads, with an average difference of 8.66°C (Appendix I, Figure 4). Due to the manual nature of the sUAS-based thermal temperature extraction and the lower resolution of the 2020 thermal flight, manual and extracted temperature values could not be compared for the 2020 flights.

4. Discussion

Differences in canopy temperature of cotton plants under four different irrigation treatments were found to negatively correlate with irrigation quantity (Appendix I, Figure 1). As the treatments became more established throughout the growing season, the observed negative correlation became more pronounced. This trend continued until the end of the season when overall atmospheric demand was reduced due to lower atmospheric temperatures as summer ended. These results aid in the validation of the described sUAS thermal setup used to collect lettuce head temperature data in the Yuma Fusarium wilt trial.

Identification of lettuce heads with Fusarium wilt symptoms was possible using thermography (Appendix I, Figures 3 & 4). Symptomatic heads were also shown to have a higher temperature using both manual IRT measurements and the sUAS thermography (Appendix I, Figure 4). Temperatures extracted from the thermal imagery, however, exhibited a higher difference between a healthy and diseased lettuce head compared to the manual IRT measurements. It should be noted that the comparisons made were of two different fields with one grown in 2020 and the other in 2021. The 2021 thermography data was taken over a field where plants exhibiting advanced stages of Fusarium wilt were removed. The thinning of diseased plants resulted in the exposure of more bare earth. Regions of exposed soil are generally hotter than regions with plants because plants actively transpire which results in lower surface temperatures through evaporative cooling. The higher exposure of hot soil can result in the perception of hotter plant temperatures due to pixel contamination. The larger the distance between the camera and the subject, the more area that is covered by a single pixel which will appear hotter if the surrounding area is contaminated by bare soil. Furthermore, the removal of diseased plants made it difficult to differentiate between diseased plants and cut stalks due to the low resolution of the thermal image.

Manually taken temperatures and those extracted from the thermal imagery show promising results. Both methods indicated higher head temperatures when comparing diseased plants to healthy ones. Manual measurements, however, are more time consuming and not feasible if trying to screen a large number of heads. The sUAS-based thermal imagery approach aims to address this problem by reducing the overall time of data collection. The lower resolution of thermal imagery makes manual comparisons using thermal imagery difficult. Setting out GCPs in the field before conducting a thermal flight would allow for accurate georeferencing of the stitched orthomosaic. Georeferenced orthomosaics also allow for automated and more accurate extractions of thermal temperatures. Automation of temperature extractions is crucial if one wants to track the spread and progression of the Fusarium wilt disease. The potential for this setup to be used as a tool for early disease detection is high as early detection of disease hotspots can help growers mitigate the spread to other parts of the field.

5. Conclusion

These results demonstrated the potential of sUAS-based thermal imagery in the detection of water stress as it is able to detect differences in canopy temperature related to differences in

irrigation. Furthermore, the study shows the potential of thermography in the detection of Fusarium wilt through differences in lettuce head temperatures. It was found that more accurate identifications were obtained in fields that had not been thinned due to pixel contamination from the surrounding soil. Future research should investigate the ability of this setup to track the development and spread of the disease. Temporal data on Fusarium wilt infection will provide more information to growers that may help mitigate the spread of the disease early in the growing season.

Appendix I

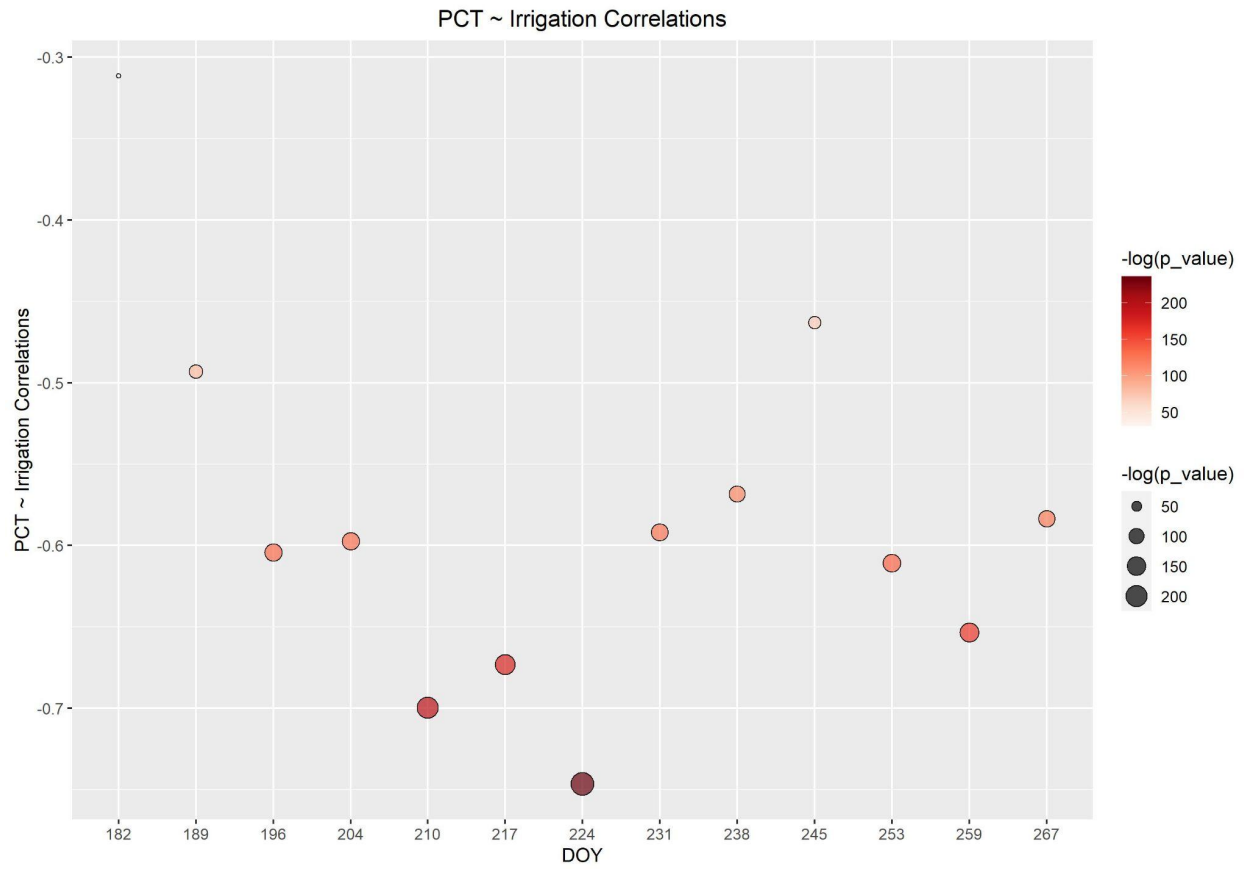


Figure 1: Correlation and significance values between plant canopy temperature (PCT) and irrigation throughout the growing season. The $-\log(p_value)$ is shown with darker colors and larger sized points representing highly significant negative correlation values.

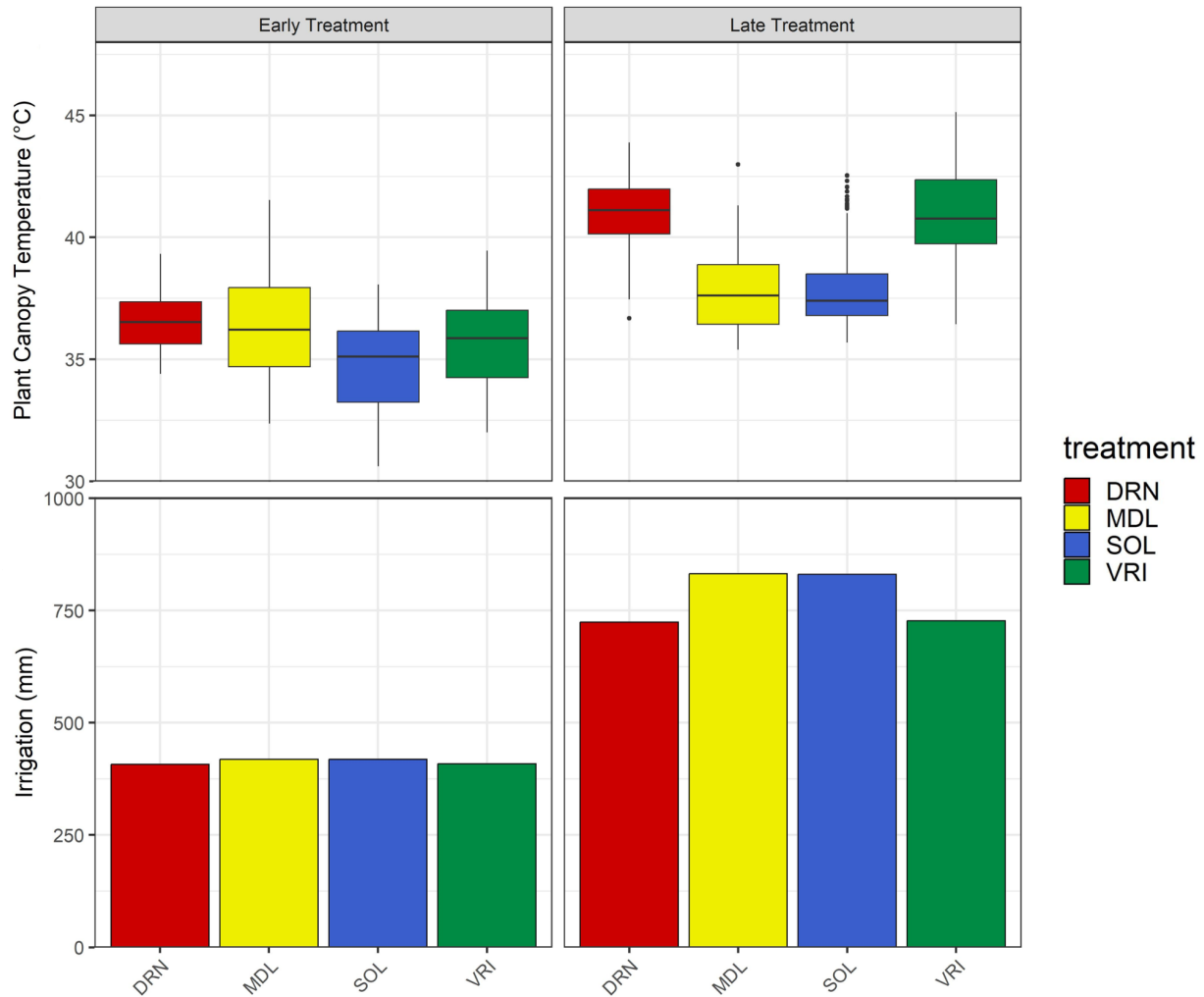


Figure 2: Canopy temperature (°C) and irrigation amount (total mm) from an early treatment and late treatment data set. The top graphs show a grouping between Drone/Variable Rate Index and Soil/Model irrigation treatments. The bottom graphs show the irrigation amount for each treatment up to the day shown. There is a large difference in irrigation amount between Done/Variable Rate Index and Soil/Model irrigation treatments. MDL, model - determined irrigation amount solely by using an FAO-56 model; VRI, variable rate index - Used VRI technology for site-specific irrigation in conjunction with the irrigation model to calculate the estimate; DRN, drone - determined irrigation amount by using FAO-56 model, but adds spatial crop cover data derived from a drone to achieve more accurate water availability estimates; SOL, soil - Used spatial data for soil water holding limits in conjunction with the model to calculate the irrigation estimate.

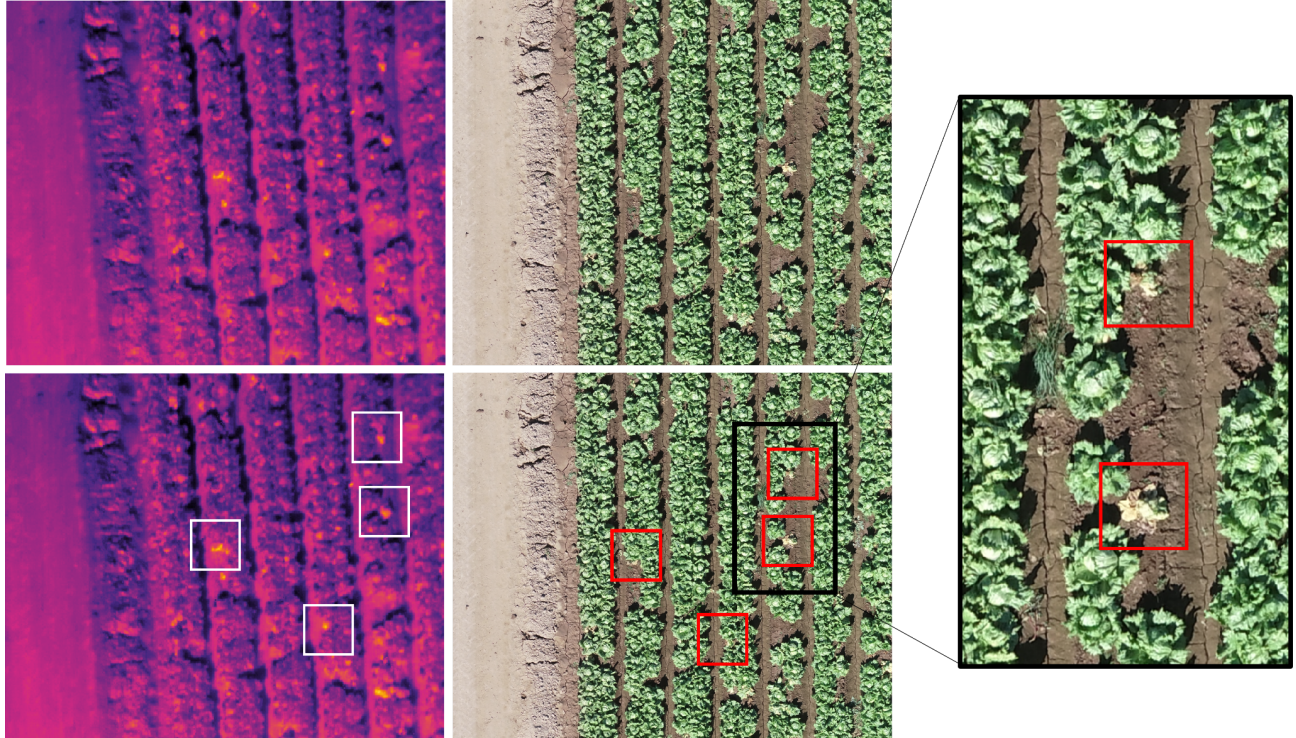


Figure 3: Identification of lettuce heads exhibiting *Fusarium* wilt symptoms using sUAS-based thermal imagery. Lettuce heads thought to be diseased are identified using thermal imagery (left; white boxes) and are confirmed using RGB imagery (right; red boxes).

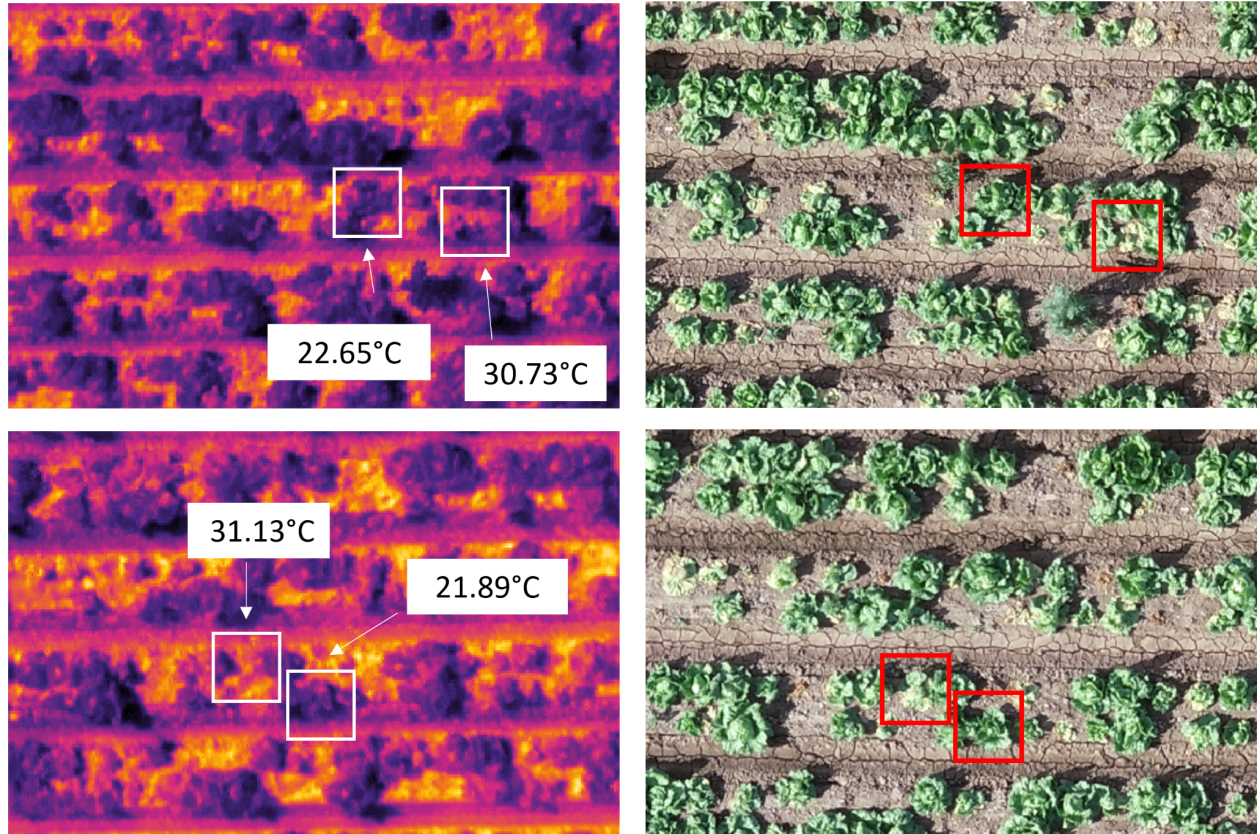


Figure 4: Comparison of plant canopy temperature values between healthy and diseased lettuce heads. Thermal imagery (left) shows that diseased lettuce heads exhibit higher plant canopy temperature values compared to healthy lettuce heads (shown in white boxes). Diseased lettuce heads are confirmed using RGB imagery (right; red boxes).

Literature Cited

- Bian, Jiang, Zhitao Zhang, Junying Chen, Haiying Chen, Chenfeng Cui, Xianwen Li, Shuobo Chen, and Qiuping Fu. 2019. "Simplified Evaluation of Cotton Water Stress Using High Resolution Unmanned Aerial Vehicle Thermal Imagery." *Remote Sensing* 11 (3): 267.
- Bradski, G. 2000. "The openCV Library." *Dr. Dobb's Journal: Software Tools for the Professional*. <https://elibrary.ru/item.asp?id=4934581>.
- Dev, Release 10 1. n.d. "Pillow (PIL Fork) Documentation." Accessed September 23, 2023. <https://media.readthedocs.org/pdf/pillow/latest/pillow.pdf>.
- Pedregosa, Fabian, Gaël Varoquaux, Alexandre Gramfort, Vincent Michel, Bertrand Thirion, Olivier Grisel, Mathieu Blondel, et al. 2012. "Scikit-Learn: Machine Learning in Python." *arXiv [cs.LG]*. arXiv. <https://www.jmlr.org/papers/volume12/pedregosa11a/pedregosa11a.pdf?ref=https://>.
- Pugh, N. A., K. R. Thorp, and E. M. Gonzalez. 2021. "Comparison of Image Georeferencing Strategies for Agricultural Applications of Small Unoccupied Aircraft Systems." *The Plant Phenome*. <https://access.onlinelibrary.wiley.com/doi/abs/10.1002/ppj2.20026>.
- Thorp, Kelly R., Sebastian Calleja, Duke Pauli, Alison L. Thompson, and Diaa Eldin Elshikha. 2022. "Agronomic Outcomes of Precision Irrigation Management Technologies with Varying Complexity." *Journal of the ASABE* 65 (1): 135–50.